TABLE I. Comparison of theoretical results [Eq. (11), $\ln(A/\delta^B)$] with empirical results [Eq. (14), $\ln(3/\delta)$].

δ^2	η	A	B	$\ln(3/\delta)$	$\ln(A/\delta^B)$
0.005	1.161 53	2.623	1.013	3.748	3.649
0.01	1.183 065	2.598	1.017	3.401	3.297
0.02	1.212 02	2.565	1.023	3.055	2.944

shortest and this distance compares well with the results of Suydam; and (c) that for stabilized experimentally observable filaments the initial size of the perturbation, b, lies between b_{opt} and $b_{op}/(1.6)^{1/2}$ (as shown in the text) explaining thereby the nearly constant size of filaments observed experimentally.

[1]S. C. Abbi and H. Mahr, Phys. Rev. Lett. 26, 604 (1971), and Appl. Phys. Lett. 19, 415 (1971).
[2]V. I. Bespalov and V. I. Talanov, Zh. Eksp. Teor. Fiz., Pis'ma 3, 471 (1966) [JETP Lett. 3, 307 (1966)].
[3]K. A. Bruckner and S. Jorna, Phys. Rev. Lett. 17, 78 (1966).
[4]B. R. Suydam, in Laser-Induced Damage in Optical Materials, U. S. National Bureau of Standards Special Publication No. 387, edited by A. J. Glass and A. H. Guenther, (U. S. GPO, Washington, D. C., 1973); B. R. Suydam, IEEE J. Quantum Electron. 10, 837 (1974).
[5]The backflow of energy into other Fourier components is neglected in this work since the perturbation is assumed to preserve its shape during propagation (aberrationless case). Inclusion of aberrations might change the results quantitatively.

Nonlinear Formulation and Efficiency Enhancement of Free-Electron Lasers

P. Sprangle, Cha-Mei Tang,[a] and W. M. Manheimer
U. S. Naval Research Laboratory, Washington, D. C. 20375
(Received 11 July 1979)

We present a general, self-consistent, nonlinear theory of the free-electron laser (FEL) process. The formulation of the temporal steady-state problem results in a set of coupled nonlinear FEL equations governing the spatial evolution of the amplitudes and wavelengths of the fields. We show that intrinsic FEL efficiencies can be greatly enhanced by spatially contouring the magnetic pump-field parameters. In the optical regime, the single-pass efficiencies are found to exceed 20%.

The operative mechanism in free-electron lasers (FEL's) is a parametric process in which a long-wavelength pump field interacts with a beam of relativistic electrons.[1-8] In this paper we take the pump to be a static, periodic, right-handed magnetic field. The frequency of the scattered radiation is given by $\omega \approx (1 + v_z c)\gamma_z^2 v_z (2\pi/l)$ $\approx 4\pi\gamma_z^2 c/l$, where $\gamma_z = (1 + v_z^2/c^2)^{-1/2}$, v_z is the axial beam velocity, and l is the pump period. The possibility of using a two-stage FEL scattering process, in order to reduce the electron energy required for very short output wavelengths, has also been suggested.[8,9]

Roughly speaking, FEL's can be divided into two categories, depending on the gain of the radiation field. In the low-gain experiments,[10] the radiation field in the interaction region increases only slightly during the passage of the electron beam, while in the high-gain experiments,[11-13] the radiation field e-folds many times in the interaction region. Hence, the low-gain regime is most appropriate for oscillator operation, while high-gain FEL's can be operated as either amplifiers or oscillators.

The main objectives of this work are to present a self-consistent nonlinear formulation of the FEL mechanism and to analyze theoretically some of the concepts necessary to develop efficient, high-power, tunable, FEL radiation sources. Some of the salient features of this theory include (i) a completely arbitrary magnetic pump field (period and amplitude can be functions of axial position), (ii) space-charge effects, (iii) arbitrary polarization of the radiation field, (iv) completely relativistic particle dynamics, and (v) frequency and spatial harmonics in the excited fields. The nonlinear formalism developed for the FEL problem is also applicable to a large class of temporal steady-state convective processes. In this approach, there is no large separation of spatial scale lengths, despite the large spatial scale difference between the wavelength of the scattered field and that of the pump field. This permits numerical solutions for cases where the electron-beam energy is extremely high. Our present treatment does not consider trapped-par-

ticle instabilities which may result in frequency sidebands about ω.

Only spatial variations along the z axis will be considered. The variable-amplitude and -period pump magnetic field can be expressed in terms of the vector potential

$$\vec{A}_0(z) = A_0(z)\{\cos[\int_0^z k_0(z')dz']\hat{e}_x + \sin[\int_0^z k_0(z')dz']\hat{e}_y\},\tag{1}$$

where the amplitude $A_0(z)$ and wave number $k_0(z)$ are known and are slowly varying functions of z. The scattered electromagnetic and electrostatic fields in terms of the vector potential $A(z,t)$ and scalar potential $\varphi(z,t)$ are taken to be

$$\vec{A}(z,t) = A_x(z)\cos[\int_0^z k_+(z')dz' - \omega t + \theta]\hat{e}_x - A_y(z)\sin[\int_0^z k_+(z')dz' - \omega t + \theta]\hat{e}_y,\tag{2a}$$

$$\varphi(z,t) = \varphi(z)\cos[\int_0^z k(z')dz' - \omega t + \theta_z],\tag{2b}$$

where the amplitudes of the potentials, $A_x(z)$, $A_y(z)$, and $\varphi(z)$, as well as the wave numbers $k_+(z)$ and $k(z)$, are slowly varying functions of z. The evolution of the scattered potentials is governed by the wave equations where the general form for the driving current is

$$\vec{J}(z,t) = -|e|n_0 v_{z0}\int_{-\infty}^{\infty}\vec{p}(t_0,t)p_z^{-1}(t_0,t)\delta(t - \tau(t_0,z))dt_0,$$

where n_0 is the uniform particle density to the left of the interaction region, i.e., $z \lesssim 0$, v_{z0} is the constant axial electron velocity at $z = 0$, $\vec{p}(t_0,t)$ is the momentum vector of the particle at time t which crossed the $z = 0$ plane at time t_0, $\tau(t_0,z) = t_0 + \int_0^z v_z^{-1}(t_0,z')dz'$ is the time it takes a particle to reach the position z if it entered the interaction region, $z = 0$, at time t_0, and $v_z(t_0,z)$ is the axial velocity of a particle at position z which was at $z = 0$ at time t_0. The reduced equations for $A_x(z)$, $A_y(z)$, $k_+(z)$ are

$$\frac{\omega^2}{c^2 - k_+^2(z)}\begin{Bmatrix} A_x(z) \\ A_y(z) \end{Bmatrix} = \pm 4|e|n_0\frac{v_{z0}}{c}\omega\int_0^{2\pi/\omega}p_z^{-1}(t_0,\tau(t_0,z))\begin{Bmatrix} p_x(t_0,\tau(t_0,z))\cos\psi(z,\tau(t_0,z)) \\ p_y(t_0,\tau(t_0,z))\sin\psi(z,\tau(t_0,z)) \end{Bmatrix}dt_0,\tag{3a}$$

$$2k_+^{1/2}(z)\frac{\partial}{\partial z}\begin{Bmatrix} A_x(z) \\ A_y(x) \end{Bmatrix}k_+^{1/2}(z)$$

$$= -4|e|n_0\frac{v_{z0}}{c}\omega\int_p^{2\pi/\omega}p_z^{-1}(t_0,\tau(t_0,z))\begin{Bmatrix} p_x(t_0,\tau(t_0,z))\sin\psi(z,\tau(t_0,z)) \\ p_y(t_0,\tau(t_0,z))\cos\psi(z,\tau(t_0,z)) \end{Bmatrix}dt_0,\tag{3b}$$

where $\psi(z,\tau) = \int_0^z k_+(z')dz' - \omega\tau + \theta$. Similar results can be obtained for $\varphi(z)$ and $k(z)$.

The particle orbits in terms of the entry time t_0 and axial position z are

$$p_x(z,\tau) = (|e|/c)[A_{0x}(z) + A_x(z,\tau)], \quad p_y(z,\tau) = (|e|/c)[A_{0y}(z) + A_y(z,\tau)],\tag{4a}$$

$$\frac{dp_z^2(z,\tau)}{dz} = -\frac{|e|^2}{c^2}\left[\frac{\partial}{\partial z}[\vec{A}_0(z) + \vec{A}(z,\tau)]^2 - 2\gamma(z,\tau)\frac{m_0c^2}{|e|}\frac{\partial}{\partial z}\varphi(z,\tau)\right],\tag{4b}$$

where $\gamma(z,\tau) = \{1 + (|e|^2/m_0^2c^4)[\vec{A}_0(z) + \vec{A}(z,\tau)]^2 + p_z^2(z,\tau)/m_0^2c^2\}^{1/2}$. At this point we take the scattered electromagnetic wave to be circularly polarized and set $A_x(z) = A_y(z) = A(z)$. Using the expressions for p_x and p_y given by Eq. (4a) in Eqs. (3a) and (3b) gives

$$\frac{\omega^2}{c^2 - k_+^2(z)}A(z) = \frac{\omega_b^2}{2c^2}m_0v_{z0}\frac{\omega}{\pi}\int_0^{2\pi/\omega}p_z^{-1}(t_0,\tau(t_0,z))[A_0(z)\cos\tilde{\psi}(z,\tau(t_0,z)) + A(z)]dt_0,\tag{5a}$$

$$2k_+^{1/2}(z)\frac{\partial}{\partial z}[A(z)k_+^{1/2}(z)] = -\frac{\omega_b^2}{2c^2}m_0v_{z0}\frac{\omega}{\pi}\int_0^{2\pi/\omega}p_z^{-1}(t_0,\tau(t_0,z))A_0(z)\sin\tilde{\psi}(z,\tau(t_0,z))dt_0,\tag{5b}$$

$$\frac{\partial\varphi(z)}{\partial z} = \frac{-\omega_b^2}{c^2}\frac{v_{z0}}{\pi}\frac{m_0c^2}{|e|}\int_0^{2\pi/\omega}\sin\psi_z(z,\tau(t_0,z))dt_0,\tag{5c}$$

$$k(z)\varphi(z) = \frac{-\omega_b^2}{c^2}\frac{v_{z0}}{\pi}\frac{m_0c^2}{|e|}\int_0^{2\pi/\omega}\cos\psi_z(z,\tau(t_0,z))dt_0,\tag{5d}$$

where $\omega_b = (4\pi |e|^2 n_0/m_0)^{1/2}$, $\psi_z(z,\tau) = \int_0^z k(z')dz'$ $- \omega\tau + \theta_z$ and $\bar{\psi}(z,\tau) = \psi(z,\tau) + \int_0^z k_0(z')dz'$. The nonlinear formulation of the FEL is fully described by Eqs. (4b) and (5). The amplitude and phase of the scattered fields as well as the axial beam momentum all vary with a characteristic axial length which is much longer than the pump wavelength l.

The ponderomotive potential plays a central role in axially bunching the electron beam. This potential is given by $\varphi_{pond}(z, \tau) = -|e|(\gamma_0 m_0 c^2)^{-1}$ $\times A_0(z)A(z) \cos\bar{\psi}(z, \tau)$, where γ_0 is the initial total gamma factor of the beam. The efficiency can be defined as the ratio of the electromagnetic-energy-flux increase to the initial electron-energy flux and is given by

$$\eta = [|e|/(m_0 c)]^2 (\omega/\omega_b^2)[v_{z0}(\gamma_0 - 1)]^{-1}$$

$$\times [k_+(z)A^2(z) - k_+(0)A^2(0)].$$

Now we present the numerical results for the coupled nonlinear FEL equations in (4b) and (5). We choose an example where the output radiation is in the optical regime. The monoenergetic electron beam enters the interaction region at $z = 0$ with a uniform density. In all of our numerical simulations a small-amplitude radiation field is introduced as a perturbation at $z = 0$.

(a) *Constant magnetic-pump illustration.*—Table I lists the salient parameters for the magnetic pump, electron beam, and output radiation. Figure 1 shows the amplitude of the vector potential of the scattered radiation, $A(z)$, and the spatial growth rate, $\Gamma = \partial[\ln A(z)]/\partial z$, as functions of z. Those plots are for an optical frequency of ω $= 2\gamma_{z0}^2 ck_0 = 2.525 \times 10^{15}$ sec^{-1}.

Figure 2 shows a comparison between the spa-

TABLE I. Optical illustration of FEL (constant magnetic-pump parameters).

Magnetic-pump parameters	
Pump wavelength l,	1.5 cm
Pump amplitude B_0,	6.0 kG
Electron beam parameters	
Beam energy E_0,	66 MeV ($\gamma_0 = 131$)
Beam current I_0,	2 kA
Axial gamma γ_{z0},	100
Beam radius r_0,	0.1 cm
Output radiation parameters	
Radiation wavelength λ,	0.75 μm
Linear e-folding length [a] L_e,	38 cm
Efficiency [a] η,	0.52%

[a] For maximum growth rate, note that $L_e = (\partial \ln A/\partial z)^{-1}$.
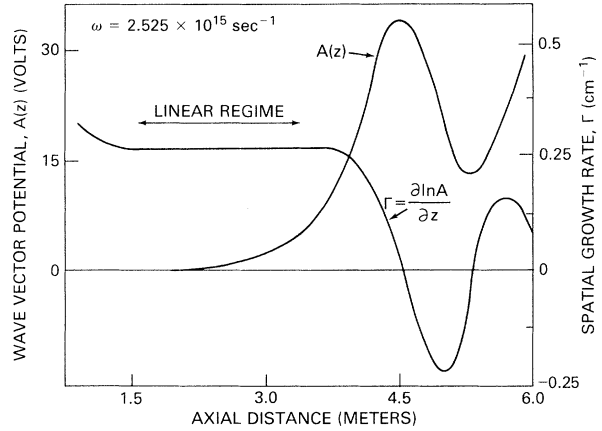
FIG. 1. Wave-vector potential $A(z)$ and spatial linear growth rate Γ as a function of axial distance in the optical regime. The frequency is chosen to give the maximum linear spatial growth rate.

tial growth rates obtained from the linear regime of the numerical simulation of our FEL equations (crosses) and the linear growth rates obtained from the dispersion relation calculated elsewhere[8, 14] (solid curve) over the frequency spectrum. Figure 2 also compares the efficiency at saturation obtained by solving the FEL equations (circles) with the calculated values of efficiency using electron trapping[7] arguments (dotted curve).

(b) *Efficiency enhancement by contouring magnetic-pump period.*[14]—The phase velocity of the total longitudinal-wave potential, i.e., ponderomotive plus space charge, is $v_{ph} = \omega/(k_+ + k_0)$. If the magnetic-pump period is held fixed, the radiation
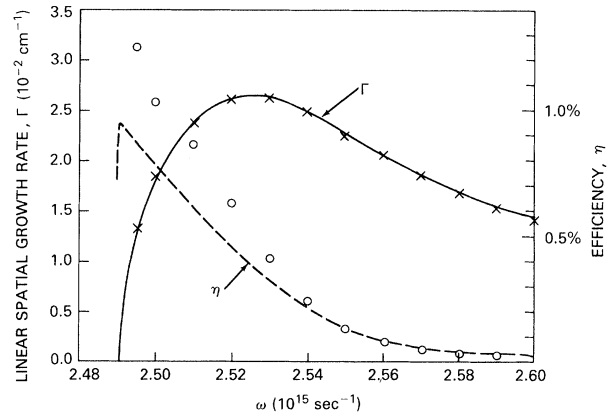
FIG. 2. A comparison of the growth rate in the linear regime of the nonlinear simulation (crosses) with the growth rate from linear theory (solid curve), and a comparison of efficiency from nonlinear theory (circles) with that from linear theory using trapping arguments (dashed curve) as a function of frequency.
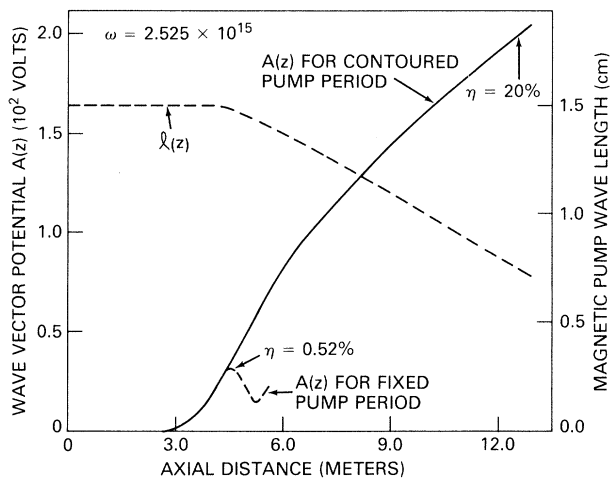
FIG. 3. Enhancement of radiation field by decreasing the magnetic-pump period. The efficiency has increased from 0.52% at $z = 4.5$ m with a constant pump period to 20% at $z = 13$ m with the period of the pump changing as shown.

field reaches its maximum value when the electrons are trapped at the bottom of the longitudinal potential wells. Just before the radiation field saturates, the electrons are somewhat spatially bunched and trapped near the bottom of the wave potential. The trapped electrons can be considered, for our purpose, to form a macroparticle. By appropriate reduction of the phase velocity as a function of axial distance down the interaction region, the longitudinal kinetic energy of this macroparticle can be further reduced and converted into wave energy. The maximum conversion efficiency obtainable by employing this scheme is $\eta_{max} = \alpha (\gamma_0 - \gamma_{0\perp})/(\gamma_0 - 1)$, where $\gamma_0 = \gamma_{0\perp}\gamma_{z0}$ and α is the fraction of particles trapped. The phase velocity must be reduced in such a way so that the inertial potential of the trapped macroparticle is always less than the potential of the growing longitudinal wave. The phase velocity can be reduced by decreasing the period of the magnetic pump[14] as a function of z. In order for the macroparticle to remain trapped, the spatial rate of change of the pump period must be sufficiently slow. Note that the pump period cannot be made arbitrarily small; for example, $l(z)$ must be greater than $2\pi r_0$ in order to ensure a pump field of the form given in (1).

A number of alternative efficiency enhancement schemes have been suggested.[15, 16] One such approach is to fix the magnetic-pump period while decreasing the magnetic-pump amplitude.[16] The maximum conversion efficiency using this method

is $\eta_{max} = \alpha (\gamma_0 - \gamma_{z0})/(\gamma_0 - 1)$. However, since $\gamma_{z0} > \gamma_{0\perp}$, it seems that the former approach would lead to higher efficiencies.

We will illustrate efficiency enhancement by contouring the pump period while holding the amplitude of the pump magnetic vector potential constant, using the parameters in Table I. The period of the magnetic pump, $l(z)$, is depicted in Fig. 3. The spatial decrease of l results in a large increase in the amplitude of the wave vector potential as shown in Fig. 3. For this particular case, the contouring is terminated at $z = 13$ m and the efficiency at this point is already 20%.

We have enjoyed stimulating discussions with I. B. Bernstein, V. L. Granatstein, and R. A. Smith. The authors would also like to acknowledge support for this work by the U. S. Defense Advanced Research Project Agency (DARPA) under Contract No. 3817, and the U. S. Office of Naval Research (ONR) under Project No. PR011-09-41.

(a)Permanent address: Jaycor, 205 South Whiting St., Alexandria, Va. 22304.

[1]J. M. J. Madey, J. Appl. Phys. 42, 1906 (1971).

[2]P. Sprangle and V. L. Granatstein, Appl. Phys. Lett. 25, 377 (1974).

[3]A. A. Kolomenskii and A. N. Lebedev, Kvantovaya Elektron (Moscow) 5, 1543 (1978) [Sov. J. Quantum Electron 8 (7), 879 (1978)].

[4]A. T. Lin and J. M. Dawson, Phys. Fluids 18, 201 (1975).

[5]F. A. Hopf, P. Meystre, M. O. Scully, and W. H. Louisell, Phys. Rev. Lett. 37, 1342 (1976), and 39, 1496(E) (1977).

[6]N. M. Kroll and W. A. McMullin, Phys. Rev. A 17, 300 (1978).

[7]P. Sprangle, R. A. Smith, and V. L. Granatstein, U. S. Naval Research Laboratory Report No. 3911, 1978 (unpublished), and in Infrared and Millimeter Waves, edited by K. Button (Academic, New York, 1979), Vol. I.

[8]P. Sprangle and R. A. Smith, U. S. Naval Research Laboratory Report No. 4033, 1979 (Phys. Rev. A, to be published).

[9]L. R. Elias, Phys. Rev. Lett. 42, 977 (1979).

[10]L. R. Elias, W. M. Fairbank, J. M. J. Madey, H. A. Schwettman, and T. I. Smith, Phys. Rev. Lett. 36, 717 (1976).

[11]V. L. Granatstein, M. Herndon, R. K. Parker, and S. P. Schlesinger, IEEE Trans. Microwave Theory Tech. 22, 1000 (1974).

[12]G. Providakes and J. Nation, J. Appl. Phys. 50, 3026 (1979).

[13]D. B. McDermott, T. C. Marshall, S. P. Schlesinger, R. K. Parker, and V. L. Granatstein, Phys. Rev. Lett.

41, 1368 (1978).

[14]P. Sprangle, Cha-Mei Tang, and W. M. Manheimer, U. S. Naval Research Laboratory Report No. 4034, 1979 (Phys. Rev. A, to be published).

[15]A. T. Lin and J. M. Dawson, Phys. Rev. Lett. 42, 1670 (1979).

[16]N. M. Kroll and M. N. Rosenbluth, private communications.